2

Optical Characterization of Elastohydrodynamic Lubrication Pressure with Surface Plasmon Resonance

C.L. Wong[1], X. Yu[2], P. Shum[3] and H.P. Ho[4]
[1]*Division of Microelectronics, School of Electrical & Electronic Engineering*
Nanyang Technological University, 50 Nanyang Drive,
[2]*Singapore Institute of Manufacturing Technology (SIMTech), 71 Nanyang Drive,*
[3]*Division of Communication Engineering, School of Electrical & Electronic Engineering*
Nanyang Technological University, 50 Nanyang Drive,
[4]*Department of Electronic Engineering, The Chinese University of Hong Kong,*
Shatin, N.T.,
[1,2,3]*Singapore*
[4]*Hong Kong*

1. Introduction

Elastohydrodynamic lubrication (EHL) is the dominant mode of lubricant in highly stressed machine elements including gears, rolling contact bearings, cams and tappets. EHL studies describe the mechanism of lubrication in highly pressurized non-conformal contacts and they contribute to the effective operation of gears and other highly stressed machine elements. Grubin and Vinogradov [1] found that the heavily loaded EHL line contacts are governed by hydrodynamics, elastic deformation of the metal surface and the lubricate viscosity variation under extreme pressure (viscosity-pressure characteristics). Theoretical studies and numerical solutions to EHL contacts have been reported by Martin [2], Downson and Higginson [3], Crook [4], Cameron and Gohar [5] and significant contributions have been made towards the complete understanding of the EHL mechanism. The theoretical revelations were later confirmed by experimental EHL techniques, especially in optical measurements. In this chapter, we review recent advances of optical techniques for EHL studies. In addition, we report the recent application of surface plasmon resonance (SPR) sensing for the imaging of EHL point contact [6-8].

2. Optical characterization of elastohydrodynamic lubrication (EHL) contacts

Optical interferometry is by far the most widely used experimental measurement method for EHL contacts. Pioneer works on optical interferometry were carried by Archard and Kirk [9, 10], Gohar, Cameron and Paul [11-13]. Archard and Kirk [9, 10] used white light to investigate the lubrication property change in crossed cylinders. The speed of the conjunction was found to be related to the colour interference fringes shift. Gohar and Cameron [11] and Cameron and Gohar [12] used the impact between a steel ball and a glass disc to generate a high

pressure micro-chamber in GPa pressure level and optical interferometry measurement was performed for the EHL lubricant film. Paul and Cameron [13] used two coherent light beams to incident on an EHL contact at two different incident angles. By analyzing the fringe orders, the refractive index and lubricant film thickness profiles were estimated.
Larsson et al. [14] applied the optical interferometry technique to investigate the pressure fluctuation when soap lumps entered a lubricated elastohydrodynamic lubrication contact. Yagi et al. [15] demonstrated the experimental study on the viscosity wedge effect in point contact EHL under high slip ratio condition. Color optical interferometry technique was applied for lubricant film thickness measurement. Nonishi et al. [16, 17] used the optical interferometry technique to study the influence of sliding on the elastohydrodynamic film. The film thickness formed between a crowned roller and a sapphire disk was measured with optical interferometry. Yang et al. [18] studied the dimple phenomena in EHL point contact formed by a glass disk and a steel ball with optical interferometry. Félix-Quinonez et al. [19] combined the optical interferometry technique with a high-speed color video camera for automatic anlaysis of interferograms, which allowed rapid imaging for the variations of interference fringe orders and film thickness. Kaneta et al. [20] used optical interferometry and Newtonian thermal EHL analyses to study the effects of the thermal conductivity of contacting surfaces on point EHL contact. They found that the distributions of pressure and film thickness were greatly affected by the velocity and slide-roll ratio. In addition, the temperature-viscosity wedge action, the heat produced by the compression work and the shearing of the lubricant were found to be the major causes of the phenomena. Jang [21] developed an image processing method for the analysis of EHL images obtained from a monochromatic optical interferometer. In their studies, interference fringe images were formed by the reflection beam from a Cr coating surface and a metal ball surface. During data processing, the interference images were converted into digital data and the interference information of the whole contacting area was collected. In the same year, Jang [22] applied the optical interferometry technique for in-situ measurement of lubrication (EHL) film, while viscosity index improver was added to the base oil. A resolution of 5nm was reported for film thickness measurement. Guo et al. [23] presented an experimental observation of a dimple-wedge elastohydrodynamic lubricating film with optical interferometry. Anomalous EHL films, a wedge shape together with a tiny dimple at the inlet region, were observed with optical interferometry in pure sliding conditions (with ultra slow speeds of 3-800 μm/s). Yang et al. [24] investigated the effect of a transversely/longitudinally oriented surface bump/groove on the lubricating performance and dimple phenomena with optical interferometry. They also obtained numerical solution of thermal EHL in the study. Wang et al. [25] used optical interferometry and theoretical analysis to study the behavior of point contact EHL films in pure rolling short stroke reciprocating motion. Jang et al. [26] modified the conventional optical interferometry technique and developed a coaxial aligning trichromatic incident light filtering system. Compared to the conventional monochromatic/dichromatic optical interferometry, their new system could provide more spectra of color components for film thickness calculation. Furthermore, the film thickness was finely digitized and nanometer scale measurement was possible. Wang and Guo et al. [27] used optical interferometry to observe the formation of abnormal EHL film with inlet-dimple in ball-on-disc and spherical roller-on-disc contacts. It was found that the inlet-dimple only appeared within a limited entrainment speed range at particular load levels, entrainment direction and kinematic condition. Kaneta et al. [28] studied the behaviors of point contact EHL films under different impact loads using optical interferometry. They also investigated

the effects of initial impact gap, impact at oily Hertzian contact and the effect of impact loading under rolling/sliding conditions. Guo et al. [29] used the optical interferometry technique to investigate the change between EHL and hydrodynamic lubrication (HL) under different entrainment speeds and applied loads. A log-log scale linear relationship was found in two lubrication regions between the film thickness and the entrainment speed (or load). In addition, they also reported the presence of a transition region, which was significantly affected by relative sliding, between these two regions. In the same year, the research group of Fu, Guo and Wong [30] further presented a stratified-layer model for the numerical analysis of optical EHL contact. The simulation results were found correlating with their previous experimental findings. Li and Guo [31] then studied the influence of spinning on EHL films under the condition of wall slippage with optical interferometry. Spin-slide ratio was introduced to represent different spinning levels and the spin-slide ratio was found to be related to the EHL film thickness, film shape, depth of inlet dimple and the speed index of the minimum film thickness. Guo and Wong et al. [32] also applied optical interferometry to identify some of the boundary slip phenomena of highly pressurized polybutenes in EHL contacts. The post-impact lateral movement of the entrapment was studied under pure rolling, pure glass block sliding and pure ball sliding conditions. Their experimental findings supported the existence of wall slippage, which was the cause of the abnormal EHL film profile with inlet dimple. Young et al. [33] studied the start-up friction behavior of EHL entrapments with optical interferometry. It was found that entrapment substantially decreased the start-up friction. The short-lived entrapment was also found providing the greatest reduction in start-up friction. Recently, the optical interferometric technique was used by Myant et al. [34] for the investigation of fluid film thickness in sliding, isoviscous elastohydrodynamic contacts (I-EHL). A monochromatic two-beam interferometer was used to measure the lubricant film thickness at different entrainment speeds and applied loads. Experimental results showed film thickness profile with a convergent wedge shape, which was believed to be responsible for the fluid pressure and load carrying capacity of the sliding contacts.

In addition to optical interferometry, other optical imaging techniques have been reported for the studies of EHL contacts in recent years. Bongaerts et al. [35] demonstrated the application of in situ confocal Raman microscopy for friction measurements in EHL contacts. Optical imaging on the EHL contact and the determination of film thickness has been demonstrated. Optical images of the contact also showed that the starvation of the contact occurred above a critical value of the product of the entrainment speed and the lubricant viscosity for single-phase aqueous Newtonian lubricants in the EHL regime. Recently, Reddyhoff et al. [36] applied the fluorescence detection technique for lubricant flow mapping in EHL contact formed between a steel ball and a glass disc. The testing lubricant was dyed with a fluorescent species. During measurement, it was illuminated with laser light and a fluorescence intensity map of the lubricant flow was produced. The fluorescence intensity results were found correlating well with conventional optical interferometric film thickness measurements under the same condition.

3. Surface plasmon resonance (SPR) imaging of EHL point contact

Ho and Wong et al. [6-8] presented the optical characterization of EHL point contact with the surface plasmon resonance (SPR) imaging technique. This technique makes use of the spectral characteristics variation associated with the SPR effect. The hydrostatic pressure inside the EHL contact causes a localized refractive index change of the lubricant. This

results in a shift of the SPR absorption dip in the spectrum, thereby producing corresponding color changes in the resultant spectral SPR image. The refractive index profile inside the entire EHL contact therefore can be imaged by the color variation in the spectral SPR image. Comparing to conventional optical interferometry, more than two order of magnitude resolution improvement has been demonstrated in the refractive index measurement inside EHL point contact [8]. In addition, the SPR imaging allows direct measurement of refractive index profile and it is unnecessary to rely on general pressure-density model. In light of these unique advantages, the SPR detection approach should be an attractive alternative for optical EHL contact characterization.

SPR imaging was first introduced by Yeatman and Ash et al. [37] and Rothenhausler and knoll [38] as a microscopy technique in late 80's. This imaging technique has further been developed for various bio-sensing applications, such as the detection of DNA [39-41], protein-protein [42], protein-carbohydrates [43] and antibody-antigen binding interactions [44-46]. Common SPR imaging approach replies on the resonance shifts in the wavelength domain and a board band light source is used for surface plasmons excitation. As described by the Fresnel model [47], a spectral absorption curve is produced by the surface plasmons excitation and the absorption dip position is related to the refractive index change in the dielectric medium. In conventional intensity based SPR imaging technique [39-43], the boardband light source is replaced by a laser source (with narrowband wavelength) and the variation of absorption dip position is transformed into corresponding intensity changes in the reflection SPR image [46]. However, the useful information in other spectral range has been neglected in this approach. Furthermore, the signal to noise ratio is found to be limited [48]. In this chapter, a novel approach of SPR imaging technique, which makes use the full spectral information in the visible range for the image formation, is presented. With a calibration curve obtained from fluids with known refractive index, the spectral variation in the spectral SPR image is further converted into corresponding two dimensional (2D) refractive index profile. This imaging technique is applied to the study of point elastohydrodynamic lubrication (EHL) contact for the 2D imaging of refractive index and pressure profile in highly pressurized EHL dimple.

3.1 Experimental set-up

An experimental set-up based on spectral SPR imaging for studying elastohydrodynamic lubricant (EHL) dimples was formed using the impact EHL microviscometer as previously described elsewhere [49-51]. The SPR imaging results were further compared with those obtained using conventional optical interferometry for refractive index determination inside the point EHL contact [52].

Formation of impact EHL dimple

As shown in **Figure 1**, the impact EHL microviscometer operates by having a steel ball impinging on a glass plate covered by a thin layer of lubricant fluid. This results in a tiny quantity of lubricant being trapped between the contacting surfaces and thus the formation of a dimple. The dimension of a typical dimple is about 300 microns in diameter and a few microns in the central film thickness. Meanwhile, the entrapped fluid dimple acts as a microscopic high pressure chamber with pressure level reaching GPa.

Spectral SPR and interference imaging system

The experimental scheme is given in **Figure 1**. Two halogen lamps with spectral range in between 400 and 850nm (emission peak at 596nm) are used as the broad band light sources

in the experiment. The optical outputs are collimated and the beam diameters are approximate 30mm. In the SPR imaging arm, a linear polarizer is used to extract the p-polarized component of the incident beam for surface plasmon excitation. Silver film (50nm) is deposited on the total internal reflection surface of a dove prism with n_d equals to 1.92 RIU. The collimated beam incidents on the sensing surface at the resonance angle (~65°). The reflection SPR image is magnified with a 10x objective lens and a CMOS imaging chip is used for image capturing. The SPR image is further processed by an image analysis program (home built) for two dimensional Hue profile extraction and processing. With the use of an experimental calibration curve, the Hue profile is further converted into corresponding refractive index distribution. During the experiment, an optical fiber spectrometer (Ocean Optics, HR2000) is used to record the SPR absorption curves for different samples. In the optical interference imaging arm, a monochromater is used to select particular wavelength from the boardband light source. At normal incident, the partial reflection beam from the silver thin film surface interferes with the reflection beam from the steel ball surface and the interferogram of the EHL dimple is formed. The interferogram is captured by another CMOS imaging chip.

3.2 Experimental results

3.2.1 EHL dimple measurement by spectral SPR imaging

PB2400 lubricant dimple

In the measurement experiment, spectral SPR imaging was applied to studying EHL dimples produced from polybutenes lubricant (PB2400). PB2400 is a high viscosity lubricant oil with a high refractive index of n_d-1.5053 RIU. The high viscosity characteristic of this lubricant may assist the formation of EHL dimple.

Spectral SPR image

As shown in the experimental configuration, by projecting a 30mm diameter beam on the EHL dimple surface, corresponding spectral SPR images were obtained and shown in **Figure 2**. **Figure 2a** is the SPR image before EHL dimple formation. We can recognize it as a pure contact between the steel ball and the glass surface. Since no SPR absorption is taking place inside the contact, the image shows the original color of the incident beam.

Figure 2b is the SPR image after EHL dimple formation. PB2400 lubricant was trapped inside the EHL dimple and experienced extremely high pressure (GPa). It changed the refractive index of the lubricant. From the SPR image, we could observe that different SPR absorptions were taking place in the dimple. The reflected color changed from the color of the incident beam to red and finally became green in color at the centre region of the dimple. As indicated in the figure, the outermost ring is believed to be the contacting region between the steel ball and the glass surface. The whole middle region is believed to be the EHL dimple trapped inside the contact. It is believed that the color variation in the SPR image is due to the increasing refractive index and corresponding shifts of SPR absorption dip. Therefore, SPR has clearly revealed the RI distribution caused by the entrapment of lubricant under EHL condition.

In **Figure 2c**, an area of the SPR image which is taken under atmosphere pressure serve as a control image. By going through the same analysis process as the dimple SPR image, it provides the uncertainty. **Figure 2d** shows the optical interferogram obtained from the EHL dimple, which was taken simultaneously during the capture of the SPR image (**Figure 2a**).

3.2.2 Image analysis of 2D spectral SPR imaging

The image coding system

In image analysis, the spectral SPR image was treated as the linear combination of three primary colors, namely red (R), green (G) and blue (B). The CIE (Commission International de I'Eclarage) defines the RGB imaging model with three standard primary components, R, G and B, which refer to the monochromatic spectral energies at wavelengths 700nm, 546.1nm and 435.8nm respectively. The color shown in an imaging pixel can therefore be represented by a linear combination of these primary components [53] (**Figure 3a**). Besides, the XYZ, CMYK, YIQ and HSV models are several most commonly used color coding systems [49, 50], which are designed to provide equivalent image representation for different engineering applications. Nevertheless, only the Hue component in the HSV coding model directly refers to the dominant wavelength of a color [54, 55]. In our experiment, the color variations in the spectral SPR image are caused by the shift of resonance absorption dip at particular wavelength, the use of Hue value thus is a more appropriate approach to represent the spectral information in the spectral SPR image.
The HSV color space model was first introduced by Smith [55] in 1978. It was originally used for the digital control of color television monitors. Hue (H), saturation (S) and value (V) are the three dimensions in the HSV color space and the hexcone model of HSV color space is shown in **Figure 3b**. **Hue (H)** refers to the color variation in the color circle. When Hue changes from 0 to 1, the colors change from red through yellow, green, blue, magenta, and back to red. **Saturation (S)** indicates the departure of a Hue from achromatic. When the saturation value varies from 0 to 1, the whiteness component of the Hue decreases. **Value (V)** refers to the departure of a Hue from black. The blackness component in the color increases, when V decreases from 1 to 0. Smith has also introduced a RGB to HSV algorithm, which given in [55], to transform colors from RGB color space model to HSV hexcone model.

Hue distribution extraction

Hue value distribution is extracted from the SPR image and shown in **Figure 4**. A 2D map of Hue is shown in **Figure 4a**. As shown in the figure, the hue values decrease from (~ 220-250 units) in the outer region to (~ 150-180 units) in the centre region. In the control image (**Figure 4b**), the standard deviation over the whole map is 1.26 units and the average value is 13 units.

3.2.3 Calibration curve

A calibration curve between the Hue values obtained from the spectral SPR image and refractive index is established with measurements on a range of lubricants and their mixtures.

SPR images

During the SPR imaging experiment, different fluid samples were coated on the silver sensor surface and the corresponding spectral SPR images were acquired and shown in **Figure 5a-5v**. SPR effect is polarization dependent and only p-polarization light suffers the SPR absorption, s-polarization can serve as a reference beam. **Figure 5a** shows the spectral SPR image, it were obtained when the polarizer was turned into p- polarization pass mode. Beside, **Figure 5b** shows the s-polarization reference image of the same surface. Various colors are shown in **Figure 5a** for different lubricant samples: PB900 (n_d – 1.4950 RIU), 5P4E (n_d – 1.6294 RIU) and PB1300 (n_d - 1.4992 RIU). No significant colour change is observed in the s-

polarization image and the spectral content resembles the original profile of the light source. This confirms that the colour variation in SPR image is due to the shift of spectral absorption profile caused by SPR effect. The SPR images of PB2400 (n_d - 1.5053 RIU) and PB 680 (n_d – 1.4903 RIU) are shown in Figure 5c and 5e respectively. In Figure 5g to 5v (except Figure 5k and 5l), the lubricant samples were obtained from the mixture of the standard lubricant samples and their refractive index values (n_d, 1.5437-1.675RIU) were measured with Abbe refractometer. The Hue values were determined by converting the RGB intensities of individual image pixels using the Hue extraction function in the MatLab program. The Hue values are plotted in the calibration curve (**Figure 7**). The Hue values are extracted from the average value within 50 x 50 pixels on the image, the standard deviation within this area provided the error bar of the data.

SPR absorption spectrum

In addition, the corresponding SPR absorption spectra were also recorded by the spectrometer. In order to remove the background spectral variation of the light source and any effect from the system spectral transfer function, each SPR spectrum was divided by the spectral obtained from the s-polarization which did not support SPR. The raw spectral plots were fitted by nine variable regression curves. SPR absorption minimums were then extracted from the fitted curves for different lubricant samples, and the corresponding plots are shown in **Figure 6**. Data shown in **Figure 6a** (n_d - 1.4903-1.5437 RIU) and **Figure 6b** (n_d - 1.5498-1.6294 RIU) reveal that the resonance minimum has moved to a longer wavelength upon increasing the refractive index. In order to determine the uncertainty of SPR resonance minimum, SPR measurements were repeated for five lubricant samples for 5 times: 5P4E (n_d – 1.6294 RIU), PB2400 (n_d - 1.5053 RIU), H 1900 (n_d -1.5052 RIU), PB 900 (n_d – 1.4950 RIU) and PB 680 (n_d – 1.4903 RIU). The uncertainty of SPR resonance minimum, which is equal to 1.2nm, is obtained from the average of five standard deviations.

Refractive index of the lubricant samples

To consider the frequency-dispersion refractive indices of the lubricants, the following equation [7] is used for the refractive indices calculation of the lubricants.

$$n_s = \sqrt{\frac{\varepsilon_m(\lambda) n_p(\lambda)^2 \sin^2\theta}{\varepsilon_m(\lambda) - n_p(\lambda)^2 \sin^2\theta}} \tag{1}$$

where n_s = refractive index of lubricant, $n_p(\lambda)$ = refractive index of glass prism as a function of wavelength, $\varepsilon_m(\lambda)$ = relative permittivity of metal film as a function of wavelength and θ = angle of incidence.

In the experiment, silver thin film is used as the sensing layer and the glass material of the dove prism is PBH72 O'Hara glass. The corresponding permittivity ε_m (λ) and refractive index n_p (λ) value can be found from the literature [57, 58]. At a fixed incident angle of 65°, the refractive index values of lubricants are calculated at particular SPR dip wavelengths.

Calibration curve

While the Hue, SPR resonance minimum values and refractive index values for standard lubricant samples have been obtained, a calibration curve can be constructed to give the relationship between Hue value and corresponding refractive index. The calibration curve is shown in **Figure 7**. This plot enables direct conversion from SPR image colour (Hue) to

refractive index value. Therefore, each single pixel in a SPR image can be converted into corresponding refractive index value. In the calibration plot, we have modified the Hue (0-255) into relative hue values (0-285). For hue values smaller or equal to 30, an additional value of 255 is added. (This modification provides us with a continuous curve in the relationship between the relative hue and SPR resonance minimum.

3.2.4 Refractive index distribution calculation

The Hue value in each pixel of **Figure 4a** is converted to spectral SPR resonance minimum value with the calibration curve (**Figure 7**). Consequently, a continuous map of resonance minimum is obtained and shown in **Figure 8a**. A standard deviation of 1.7nm and an average value of 491.2nm are recorded in the control image (**Figure 8b**). Finally, the SPR resonance minimum maps are further converted to corresponding RI distributions with the help of the calibration curve and they are shown in **Figure 8c and 8d**. Only a small increase in refractive index is found in the outermost region of the dimple, which corresponds to the contact zone between the steel ball and the glass surface. However, a much larger refractive index increase is found near the centre region of the dimple. Using a RI value of 1.4664 RIU for PB 2400 lubricant at atmospheric pressure, the Hue value obtained from the centre of the dimple, where the pressure is at its maximum, the RI value has increased by 5.3% to 1.5447 RIU. In the control image, the average value over the map is 1.47 RIU, which corresponds to the refractive index value of PB 2400 lubricant at atmosphere pressure. In addition, the standard deviation value in the map also gives us the error bar of the detection, which is 0.00079 RIU. The centre region of an EHL dimple acts as a microscopic high pressure chamber with pressure level reaching the order of GPa. Therefore, the molecular density and corresponding refractive index of the entrapped fluid are increased.

3.2.5 Pressure distribution

Figure 9 shows the experimental pressure-refractive index relationship of PB 2400 lubricant that we previous reported in [6]. From this plot, the refractive index map can be further converted to pressure map of the EHL dimple. The corresponding 2-D pressure map as converted using this plot is shown in **Figure 10a**. As shown in the figure, a rapid increase of pressure (maximum of 0.76 GPa pressure) is observed in the center part of the EHL dimple. In the control image (Figure 5.10b), the measured pressure variation over the surface is equal to 0.0024 GPa, which indicates the measurement uncertainty of the system. In addition, the average value is found to be 0.158 GPa. This represents the baseline drift of the system. We have also done the measurements with other lubricants besides PB2400. Measurements on EHL dimple produced with another kind of high viscosity lubricant H1900 (n_d -1.5052 RIU) have been carried out also. Experimental results from H1900 agree with the findings in PB2400 dimple.

3.2.6 Sensitivity estimation

As reported in [59, 46], the sensitivity and resolution of a SPR sensor can be calculated from the following equations,

$$S = \Delta x / \Delta n_s \tag{2}$$

$$R = S \cdot U \tag{3}$$

where S and *R* are the sensitivity and resolution respectively, Δx is the sensor response and *U* is the measurement uncertainty.

The calibration plot (**Figure 7**) shows the Hue value response (ΔHue) in spectral SPR image for particular refractive index variations (Δn_s). As shown in **Figure 7**, ΔHue = 120.6 units is measured in between 1.5656 and 1.4609 RIU. From equation (2), the system sensitivity is found to be 8.7 $\times 10^{-4}$ (RIU/Hue unit). For the standard deviation in PB 2400 lubricant measurement (1.08 Hue units) is used as the measurement uncertainly, the detection resolution of the spectral SPR imaging technique is found to be 9.4 $\times$ 10^{-4} RIU.

4. Comparison with optical interferometry

As described in section 2, optical interferometry is by far the most widely used measurement technique for EHL contacts [9-34]. Wong and Guo et al. [52] presented the measurement of the refractive index of a liquid lubricant at high pressure within an EHL impact dimple using optical interferometry technique. An accuracy of ±10% in refractive index determination (resolution of 0.17 RIU) was achieved. **Table 1** compares the refractive index measurement resolution between spectral SPR imaging and optical interferometry technique. Experimental results show that the SPR techniques can provide more than 180 times resolution improvement over the conventional technique in refractive determination inside the EHL dimple. The spectral SPR imaging technique is based on the shift of the resonance minimum in the spectral curve. As indicated by **Figure 6b**, a change as low as 0.06 RIU in refractive index value causes a shift of over 100nm in the SPR dip. Meanwhile a relatively low measurement uncertainty of 1.2nm has been demonstrated.

In conventional optical interferometry, the interference fringe pattern image cannot provide pixel-wise two-dimensional RI mapping for the EHL contact, which means that some information has been excluded. On the other hand, spectral SPR imaging offers complete information related to the two dimensional RI distribution of an EHL dimple. With known pressure-refractive index relations, one can readily obtain *in situ* pressure mapping for EHL dimple.

In conclusion, the spectral SPR imaging technique has overcome several major detection shortcomings of current measurement techniques for studying EHL. In addition, ,significant improvement in measurement resolution has been demonstrated.

	Optical Interferometry	Spectral SPR Imaging sensor
Resolution	0.17 RIU	9.4 x 10^{-4} RIU
Resolution Improvement	-----	181 times
		2D RI mapping

Table 1. Measurement resolution comparison between spectral SPR image and optical interferometry.

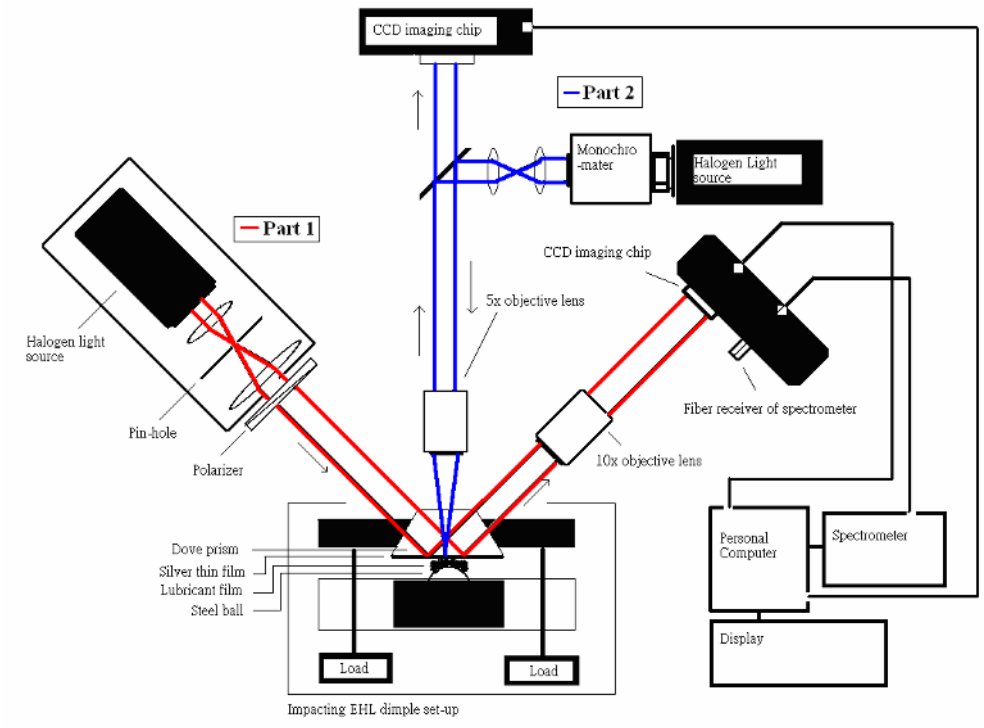

Fig. 1. Experimental scheme of the EHL dimple detection with spectral SPR sensing technique. Part 1 is the spectral SPR imaging set up (the red optical path) and part 2 is the conventional optical interferometry set up (the blue optical path).

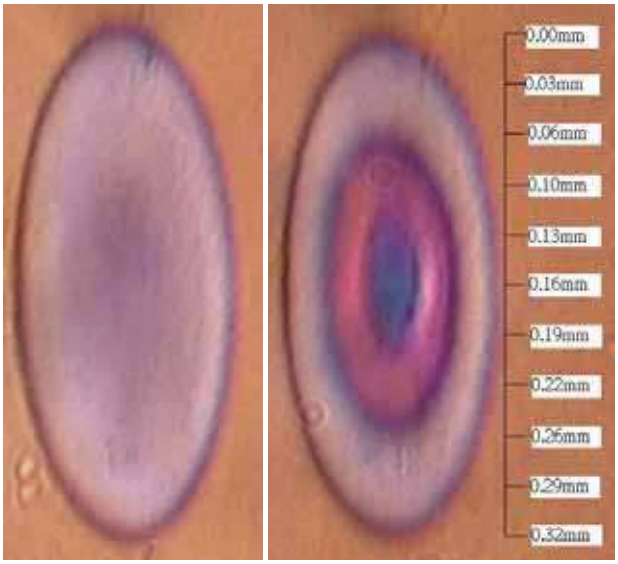
0.00mm
0.03mm
0.06mm
0.10mm
0.13mm
0.16mm
0.19mm
0.22mm
0.26mm
0.29mm
0.32mm

(a) (b)

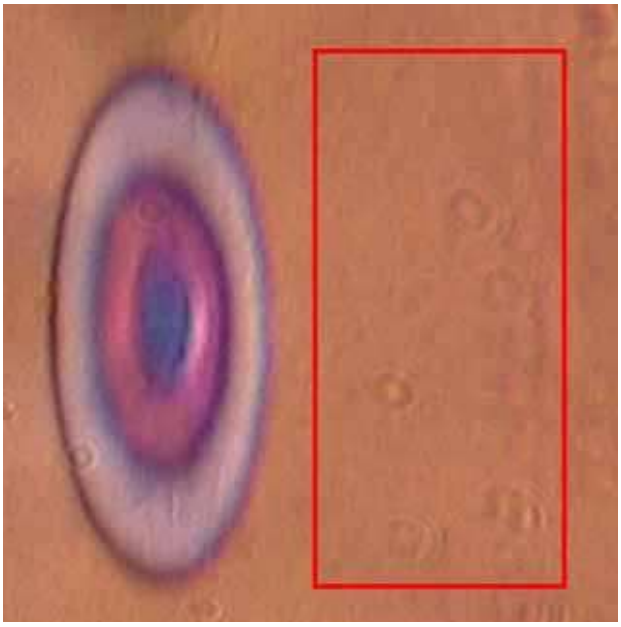

(c)

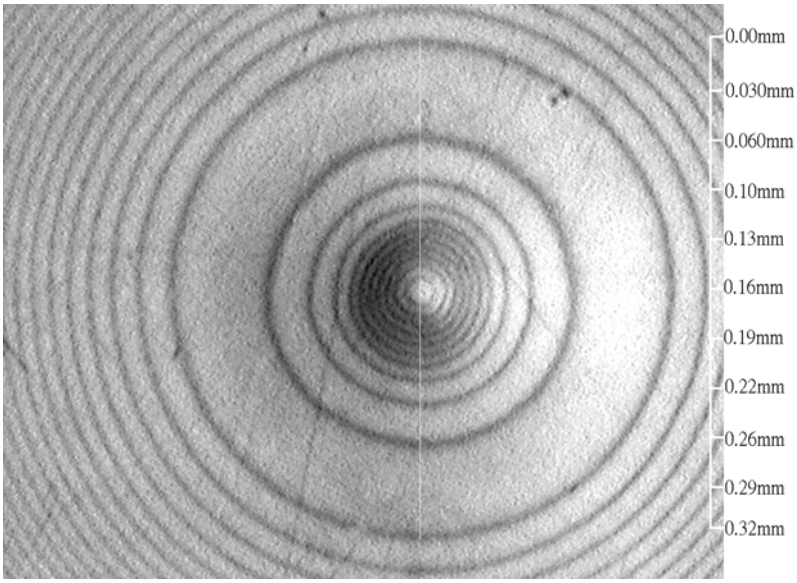

(d)

Fig. 2. Spectral SPR imaging of lubricant PB 2400 dimple: a) Image before dimple production, b) Image after dimple formation c) Image obtained under atmosphere pressure (control image). d) Optical interference image of the EHL dimple.

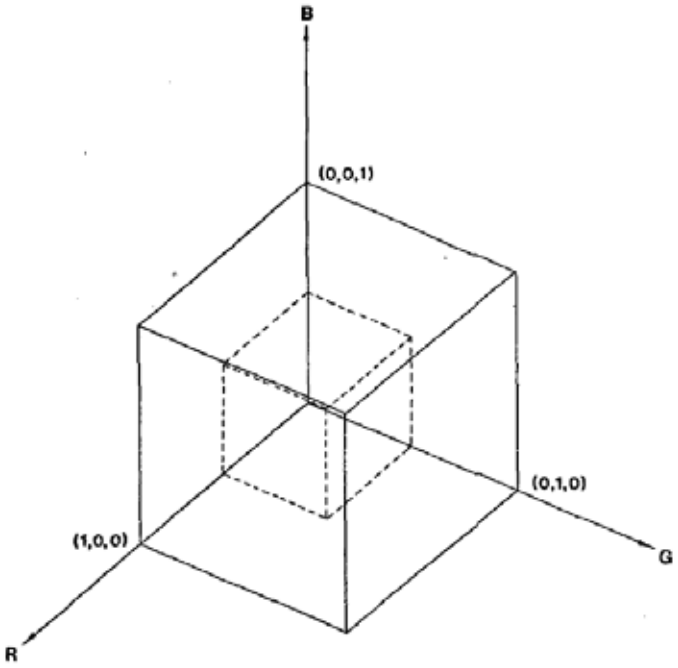

(a)

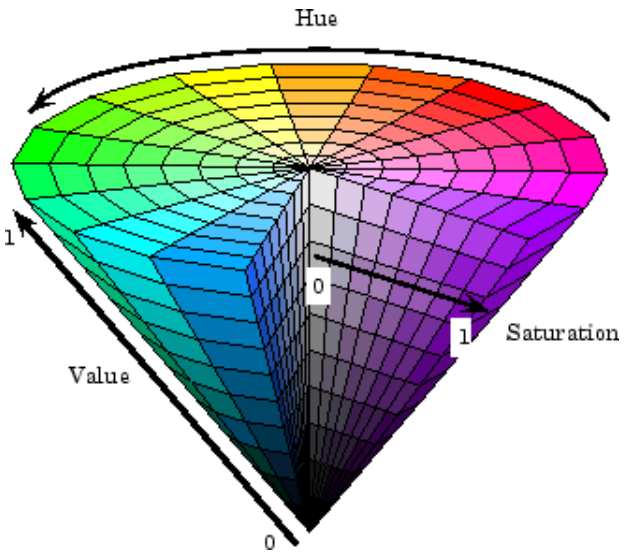

(b)

Fig. 3. a) RGB colorcube model [53], b) HSV hexcone model [56].

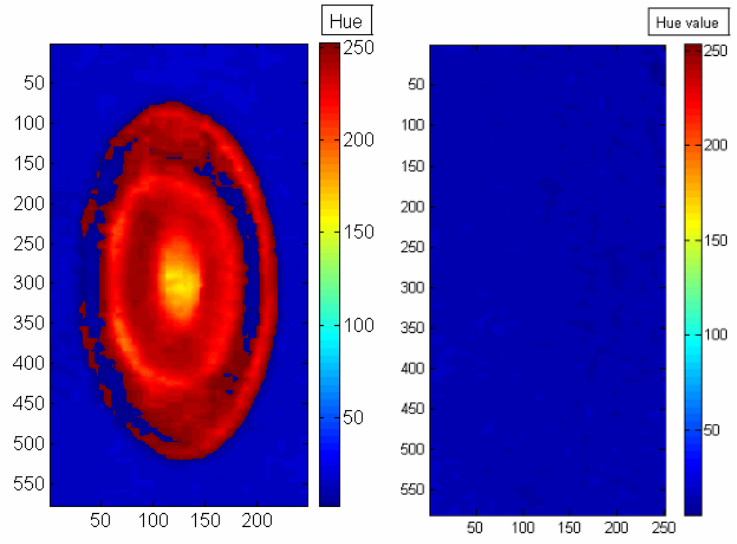

Fig. 4. a) Hue profile of lubricant PB 2400 dimple, b) Hue profile of control image

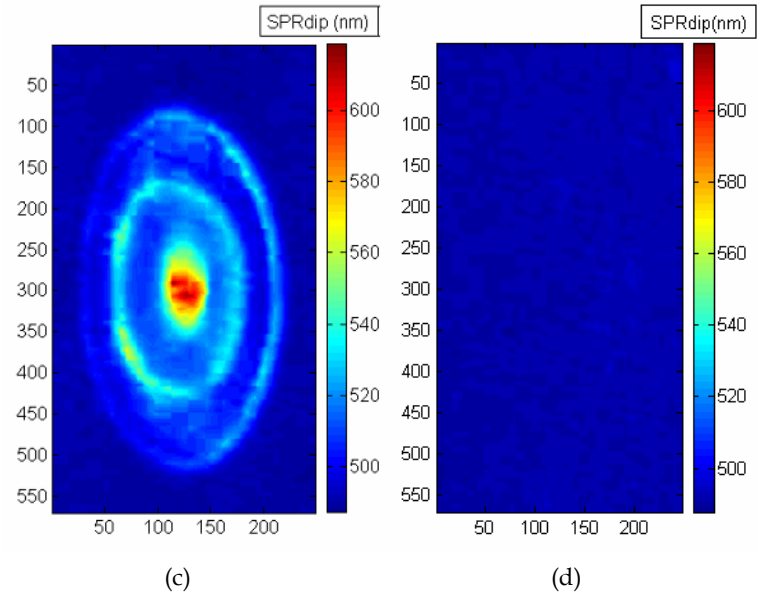

Fig. 4. c) SPR wavelength minimum profile of lubricant PB 2400 dimple d) SPR wavelength minimum profile of control image.

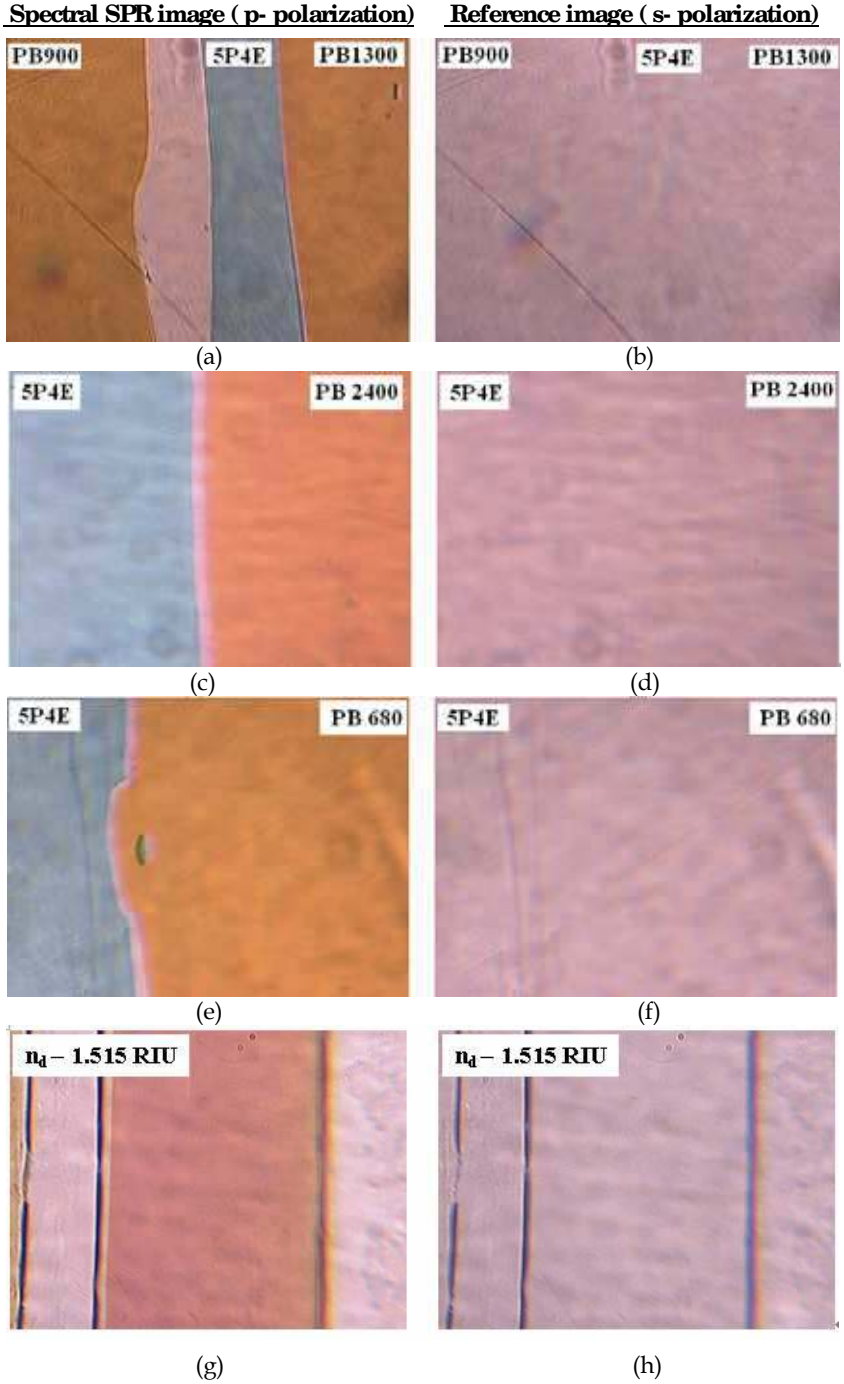
Spectral SPR image (p- polarization)
Reference image (s- polarization)
PB900
5P4E
PB1300
(a)
(b)
5P4E
PB 2400
(c)
(d)
5P4E
PB 680
(e)
(f)
n_d – 1.515 RIU
(g)
(h)

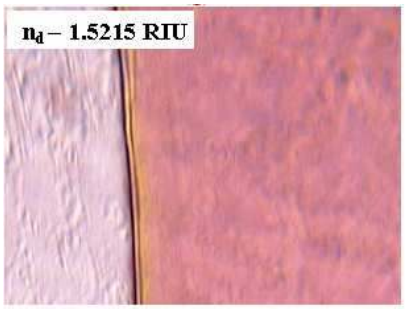
n_d – 1.5215 RIU

(i)

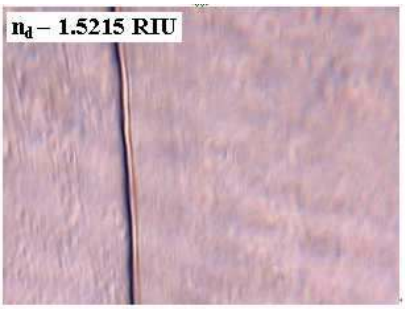
n_d – 1.5215 RIU

(j)

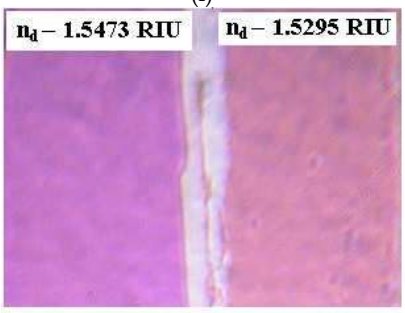
n_d – 1.5473 RIU
n_d – 1.5295 RIU

(k)

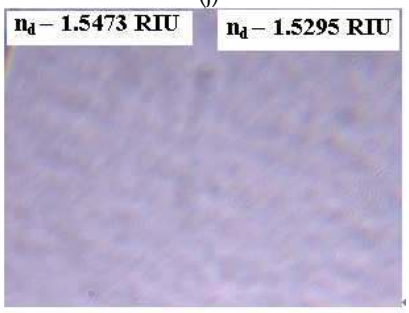
n_d – 1.5473 RIU
n_d – 1.5295 RIU

(l)

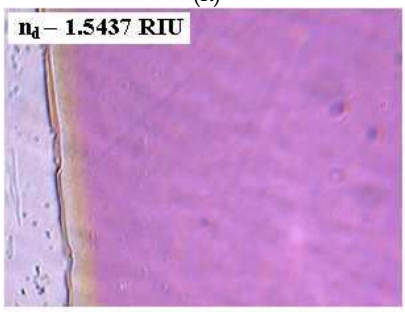
n_d – 1.5437 RIU

(m)

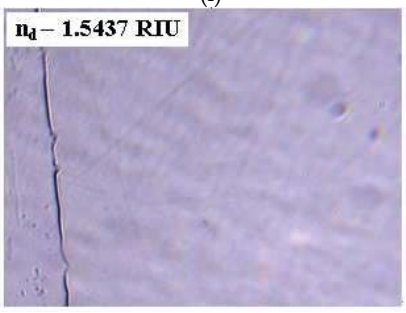
n_d – 1.5437 RIU

(n)

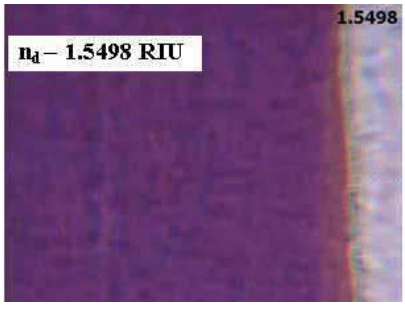
1.5498
n_d – 1.5498 RIU

(o)

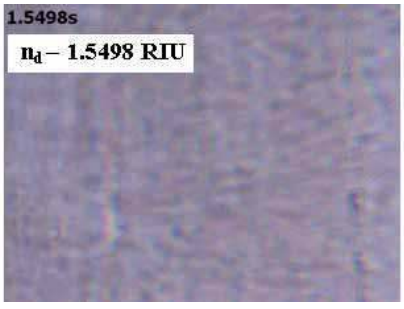
1.5498s
n_d – 1.5498 RIU

(p)

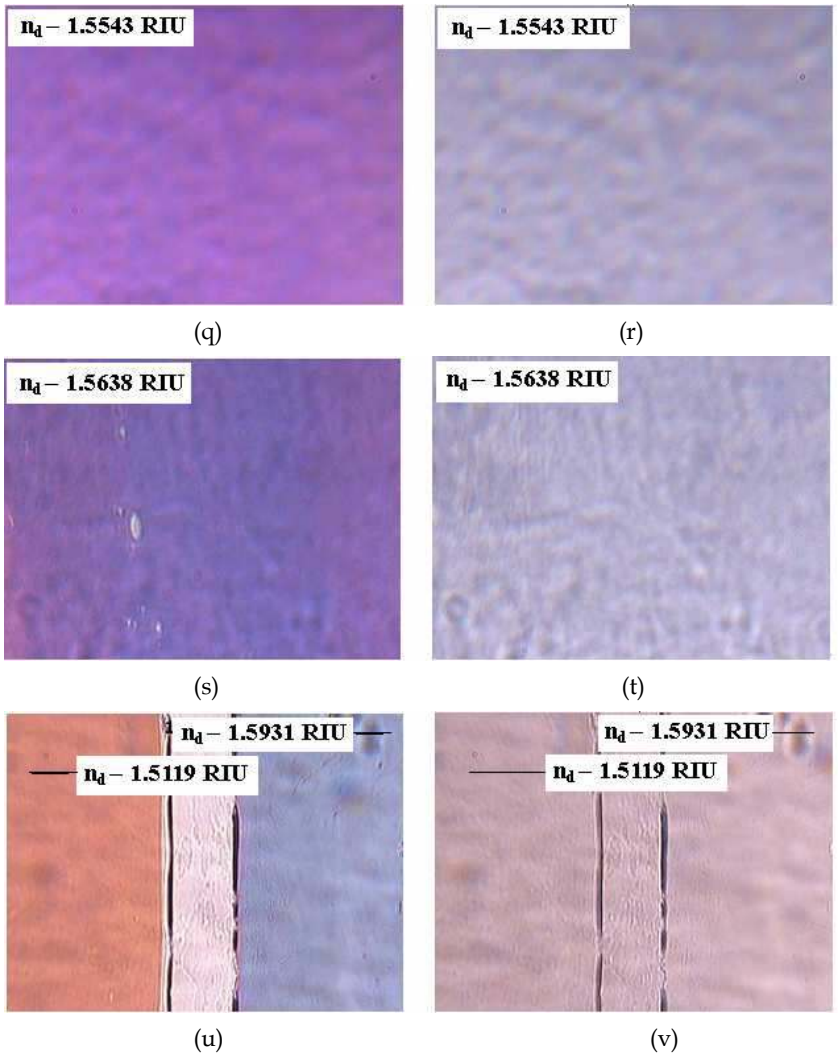

Fig. 5. Spectral SPR images obtained from lubricant samples with known refractive index values for calibration. PB 900 (n_d – 1.4950 RIU), 5P4E (n_d – 1.6294 RIU), PB1300 (n_d - 1.4992 RIU), PB2400 (n_d - 1.5053 RIU) and PB 680 (n_d – 1.4903 RIU). In g)-v) (expect k) and l)), the lubricant samples are obtained from the mixture of the standard lubricant samples and their refractive index values (n_d, 1.5437-1.675RIU) were measured with Abbe refractometer.

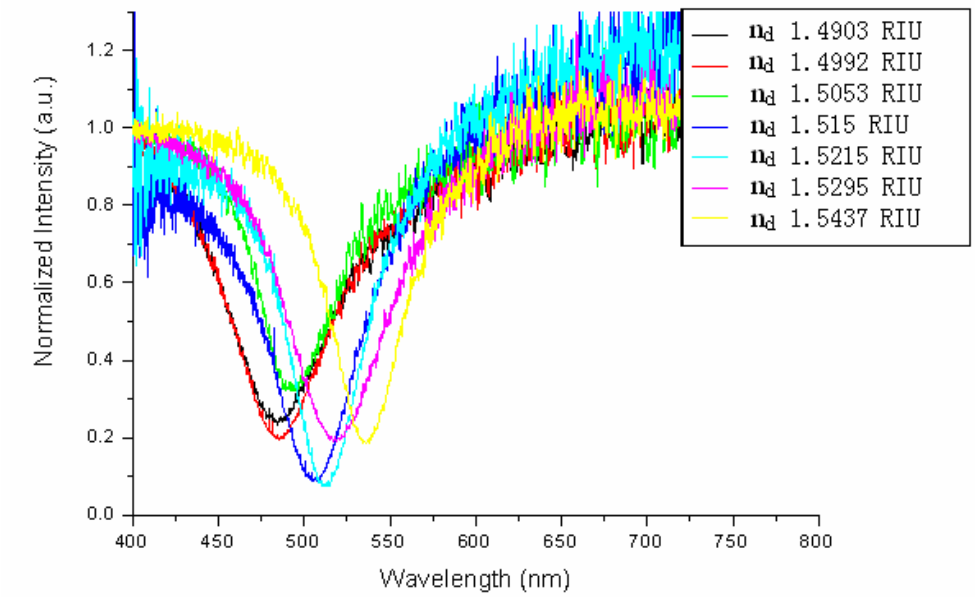

(a)

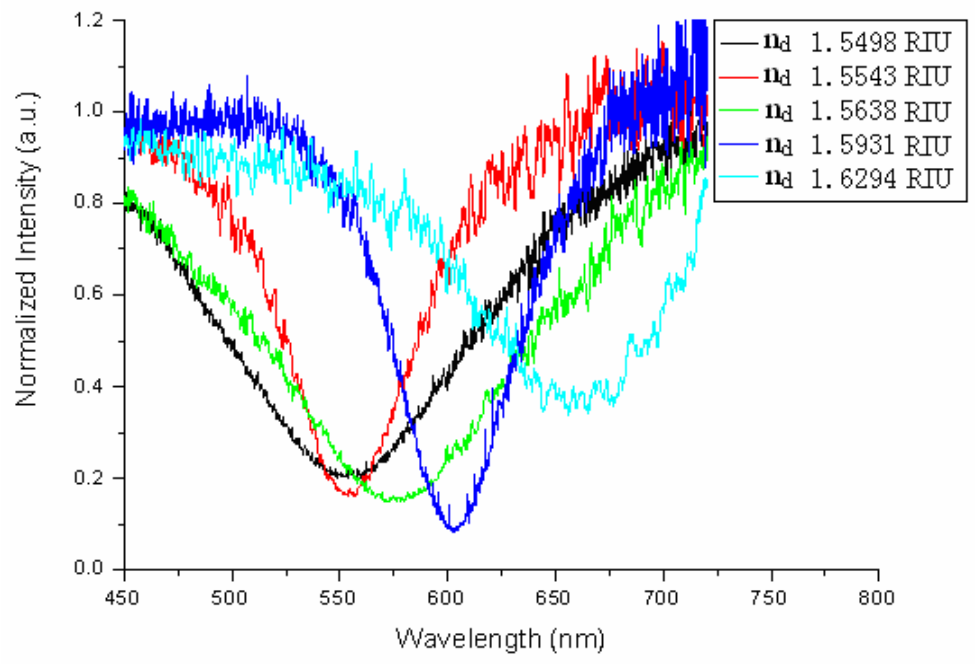

(b)

Fig. 6. SPR absorption spectra of lubricant samples for calibration.

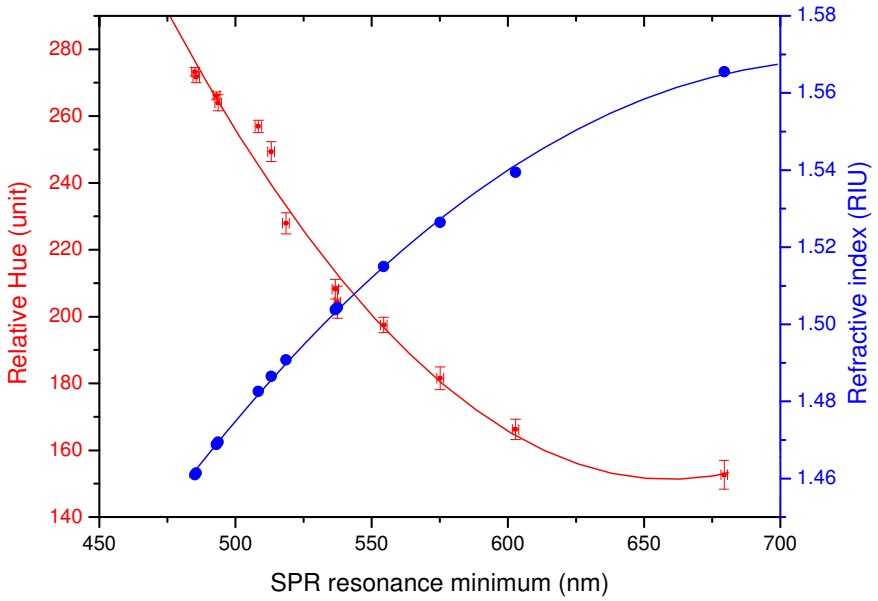

Fig. 7. Calibration curve for image conversion from refractive index value.

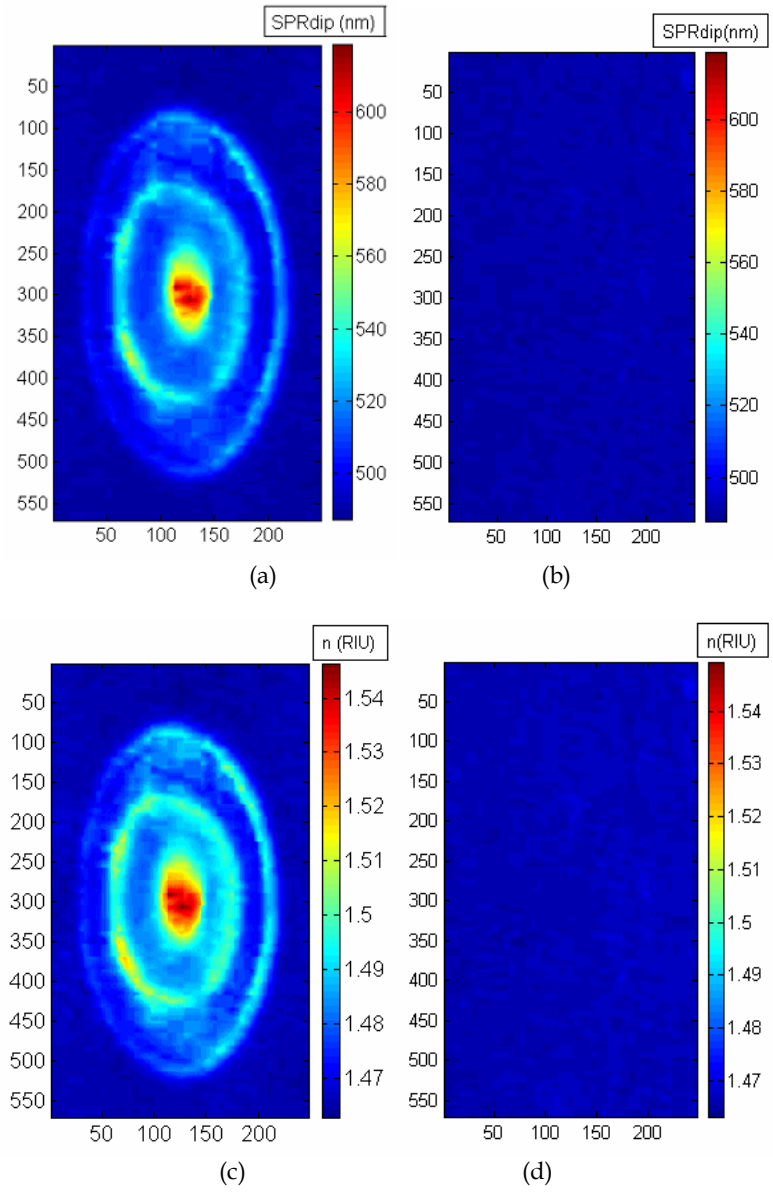

Fig. 8 a) SPR wavelength minimum profile of lubricant PB 2400 dimple b) SPR wavelength minimum profile of control image c) Refractive index profile of lubricant PB 2400 dimple d) Refractive index profile of control image.

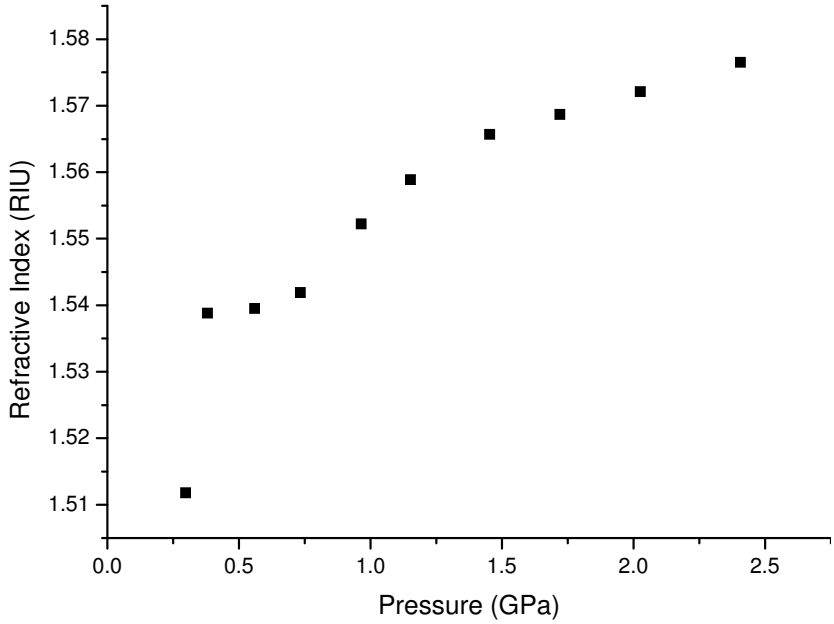

Fig. 9. Pressure – refractive index relation of lubricant PB 2400 [6].

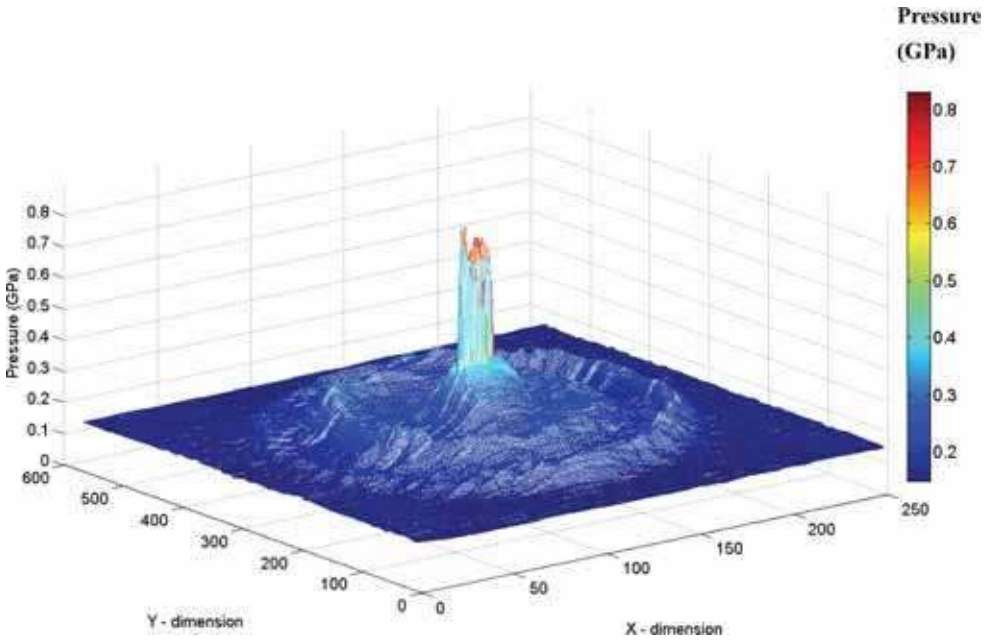

(a)

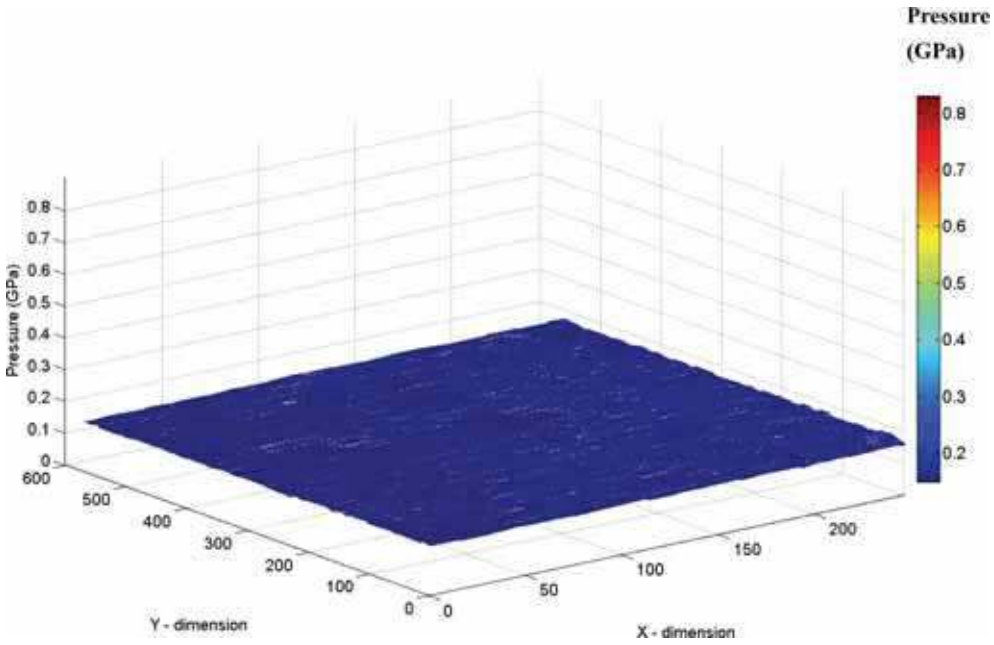

b)

Fig. 10. a) Pressure profile of lubricant PB 2400 dimple, b) Pressure profile of control image.

5. Reference

[1] A.N. Grubin and I.E. Vinogradova, Central Scientific Research Insfitute for Technology and Mechanicul Engineering 30, Moscow, (1949). (DSIR Translation No. 337).

[2] H.M. Martin, Lubrication of gear teeth, London 102, pp.199, (1916).

[3] D. Dowson and G.R. Higginson, Elastohydrodynamic Lubrication, Pergamon Press, Oxford, (1977).

[4] A.W. Crook, Electohydrodynamic Lubrication of rollers, Nature 190, pp. 1182, (1961).

[5] A. Cameron and R. Gohar, Optical measurement of oil film thickness under electo-hydrodynamic Lubrication, Nature 200, pp. 458-459, (1963).

[6] C.L. Wong, H.P. Ho, K.S. Chan, and S.Y. Wu, Application of surface plasmon resonance sensing to studying elastohydrodynamic lubricant films, Applied Optics 44, pp. 4830-4837, (2005).

[7] H.P. Ho, C.L. Wong, K.S. Chan, S.Y. Wu and C. Lin, Application of 2-D spectral surface plasmon resonance to the imaging of pressure distribution in elastohydrodynamic (EHD) lubricant films, Applied Optics 45, pp. 5819-5826, (2006).

[8] C.L. Wong, H.P. Ho, K.S. Chan, P.L. Wong, S.Y. Wu, C. Lin, Optical characterization of elastohydrodynamic lubricated (EHL) contacts using surface plasmon resonance (SPR) effect, Tribology International 41(5), pp. 356-366, (2008).

[9] J.F. Archard and M.T. Kirk, Lubrication at point contacts, Proc. R. Sot. London, Ser. A 261, pp. 532-550, (1961).

[10] J.F. Archard and M.T. Kirk, Influence of elastic modulus on the lubrication of point contacts, Proc. Lubrication and Wear Convention, Inst. Mech. Eng., London 15, pp. 18 l-189, (1963).

[11] R. Gohar and A. Cameron, The mapping of elastohydrodynamic contacts, ASLE Trans., pp. 215-225, (1966).

[12] A. Cameron and R. Gohar, Theoretical and experimental studies of the oil film in lubricated point contact, Proc. R. Sot. London, Ser. A 291, pp. 520-536, (1966).

[13] G.R. Paul and A. Cameron, An absolute high-pressure microvisometer based on refractive index. Proc. R. Soc. A 331, pp. 171-84, (1972).

[14] P.O. Larsson, R. Larsson, A. Jolkin, O. Marklund, Pressure fluctuations as grease soaps pass through an EHL contact, Tribology International 33 (3-4), pp. 211-216, (2000).

[15] K. Yagi, , K. Kyogoku, T. Nakahara, Temperature measurements of oil film and surface in point contact EHL under high slip ratio conditions, Japanese Journal of Tribology 46 (5), pp. 290-291, (2001).

[16] T. Nonishi, S. Oda, Decrease of elastohydrodynamic minimum film thickness with increase of a slide, Japanese Journal of Tribology 46 (1), pp. 53-55, (2001).

[17] T. Nonishi, S. Oda, Decrease of Elastohydrodynamic Minimum Film Thickness with Increase of a Slide, Toraibarojisuto/Journal of Japanese Society of Tribologists 46 (2), pp. 171-177, (2003).

[18] P. Yang, M. Kaneta, S. Masuda, Quantitative comparisons between measured and solved EHL dimples in point contacts, Journal of Tribology 125 (1), pp. 210-214, (2003).

[19] A. Félix-Quinonez, P. Ehret, J.L. Summers, New experimental results of a single ridge passing through an EHL Conjunction, Journal of Tribology 125 (2), pp. 252-259, (2003).
[20] M. Kaneta, P. Yang, Effects of thermal conductivity of contacting surfaces on point EHL contacts, Journal of Tribology 125 (4), pp. 731-738, (2003).
[21] S. Jang, Monochromatic image analysis of elastohydrodynamic lubrication film thickness by fringe intensity computation, KSME International Journal 17 (11), pp. 1704-1713, (2003).
[22] S. Jang, Experimental study on the shear thinning effects of viscosity index improver added lubricant by in-situ optical viscometer, Korea Australia Rheology Journal 15 (3), pp. 117-124, (2003).
[23] F. Guo, P.L. Wong, Experimental observation of a dimple-wedge elastohydrodynamic lubricating film, Tribology International 37 (2), pp. 119-127, (2004).
[24] P. Yang, J. Cui, M. Kaneta, H. Nishikawa, Influence of a surface bump or groove on the lubricating performance and dimple phenomena in simple sliding point EHL contacts, Journal of Tribology 126 (3), pp. 466-472, (2004).
[25] J. Wang, T. Hashimoto, H. Nishikawa, M. Kaneta, Pure rolling elastohydrodynamic lubrication of short stroke reciprocating motion, Tribology International 38 (11-12 SPEC. ISS.), pp. 1013-1021, (2005).
[26] S.Y. Jang, H.S. Kong, A study on the monitoring of nano scale EHL film formation with ultra low aspect ratio, Key Engineering Materials 297-300 I, pp. 257-262, (2005).
[27] X.F. Wang, F. Guo, Z.X. Fu, P.R.Yang, Experimental study of an abnormal EHL film with inlet-dimples, Mocaxue Xuebao/Tribology 27 (3), pp. 269-273, (2007).
[28] M. Kaneta, S. Ozaki, H. Nishikawa, F. Guo, Effects of impact loads on point contact elastohydrodynamic lubrication films, Proceedings of the Institution of Mechanical Engineers, Part J: Journal of Engineering Tribology 221 (3), pp. 271-278, (2007).
[29] F. Guo, Z. Fu, P.L. Wong, P. Yang, Experimental study on lubrication regime variation in point contacts, Tribology International 41 (6), pp. 451-460, (2008).
[30] Z. Fu, F. Guo, P.L. Wong, Theoretical study on the interferometry of thin EHL film measurement, Tribology Letters 31 (1), pp. 57-65, (2008).
[31] X.M. Li, F. Guo, Influence of spinning on elastohydrodynamic lubrication film with wall slippage, Mocaxue Xuebao/Tribology 29 (2), pp. 123-127, (2009).
[32] F. Guo, P.L. Wong, M. Geng, M. Kaneta, Occurrence of wall slip in elastohydrodynamic lubrication contacts, Tribology Letters 34 (2), pp. 103-111, (2009).
[33] A. Young, S. Bair, Experimental investigation of friction in entrapped elastohydrodynamic contacts, Tribology International 43 (9), pp. 1615-1619, (2010).
[34] C. Myant, M. Fowell, H.A. Spikes, J.R. Stokes, An investigation of lubricant film thickness in sliding compliant contacts, Tribology Transactions 53 (5), pp. 684-694, (2010).
[35] J.H.H. Bongaerts, J.P.R. Day, C. Marriott, P.D.A. Pudney, A.M. Williamson, In situ confocal Raman spectroscopy of lubricants in a soft elastohydrodynamic tribological contact, Journal of Applied Physics 104 (1), art. no. 014913, (2008).

[36] T. Reddyhoff, J.H. Choo, H.A. Spikes, R.P. Glovnea, Lubricant Flow in an Elastohydrodynamic Contact Using Fluorescence, Tribology Letters 38, pp. 207–215 (2010).
[37] E. Yeatman and E. Ash, Surface plasmon microscopy, Electronics Letters 23, pp. 1091, (1987).
[38] B. Rothenhäusler and W. Knoll, Surface-plasmon microscopy, Nature 332, pp. 615, (1988).
[39] E.A. Smith, M.G. Erickson, A.T. Ulijasz, B. Weisblum and R.M. Corn, Surface plasmon resonance imaging of transcription factor proteins: interactions of bacterial response regulators with DNA arrays on gold films, Langmuir 19, pp. 1486–1492, (2003).
[40] E.A. Smith, M. Kyo, H. Kumasawa, K. Nakatani, I. Saito and R.M. Corn, Chemically induced hairpin formulation in DNA monolayers, Journal of the American Chemical Society 124, pp. 6810–6811, (2002).
[41] H.J. Lee, T.T. Goodrich and R.M. Corn, SPR imaging measurement of 1-D and 2-D DNA microarrays created from microfluidic channels on gold thin films, Analytical Chemistry 73, pp. 5525–5531, (2001).
[42] G.J. Wegner, H.J. Lee, G. Marriott and R.M. Corn, Fabrication of histidine-tagged fusion protein arrays for surface plasmon resonance imaging studies of protein-protein and protein-DNA interactions, Analytical Chemistry 75, pp. 4740–4746, (2003).
[43] E.A. Smith, W.D. Thomas, L.L. Kiessling and R.M. Corn, Surface plasmon resonance imaging studies of protein-carbohydrate interactions, Journal of the American Chemical Society 125, pp. 6140–6148, (2003).
[44] C.L. Wong, H.P. Ho, Y.K. Suen, S.K. Kong, Q.L. Chen, W. Yuan, S.Y. Wu, Real-time protein biosensor arrays based on surface plasmon resonance differential phase imaging, Biosensors and Bioelecrtonics 24 (4), 606-612 (2008).
[45] C.L. Wong, H.P. Ho, T.T. Yu, Y.K. Suen, W.W.Y. Chow, S.Y. Wu, W.C. Law, W. Yuan, W.J. Li, S.K. Kong, and C. Lin, Two-dimensional biosensor arrays based on surface plasmon resonance phase imaging, Applied Optics 46, 2325-2332 (2007).
[46] C.L. Wong, Imaging surface plasmon resonance (SPR) photonic sensors, Thesis (Ph.D.), The City University of Hong Kong, 2007.
[47] P. Yeh, Optical waves in layered media, Wiley, New York, (1988).
[48] J. Homola, H. Vaisocherová, J. Dostálek, M. Piliarik, Multi-analyte surface plasmon resonance biosensing, Methods 37 (1), 26–36 (2005).
[49] P.L. Wong, S. Lingard and A. Cameron, A simplified impact microviscometer, Tribology International 25 (6), pp 363-366, (1992).
[50] R. Gohar and A. Cameron, The mapping of elastohydrodynamic contacts, ASLE Transaction 10, pp. 215–225, (1966).
[51] A. Cameron and R. Gohar, Theoretical and experimental studies of the oil film in lubricated point contact, In: Proc. R. Soc. London, Ser. A 291, pp. 520–536, (1966).
[52] P.L. Wong, F. Guo and C. Feng, The measurement of the refractive index of a liquid lubricant at high pressure within an EHL impact dimple using a single optical interferogram, Tribology International 36 (7), pp. 497-504, (2003).

[53] F.V.D. Heijden, Image Based Measurement system, John Wiley & Sons, pp. 76-77, (1994).
[54] T. Bose, Digital signal and image processing, Wiley, pp. 606-609, (2004).
[55] A.R. Smith, Color gamut transform pairs, Computer Graphics 12(3), pp. 12-19, (1978).
[56] Matlab image processing toolbox, http://www.mathworks.com/access/helpdesk/help/toolbox/images/f8-22706.html.
[57] E.D. Palik, Handbook of Optical Constants of Solids, Academic, pp. 275–358, (1985).
[58] Department of Applied and Computer Optics of the St. Petersburg State Institute of Fine Mechanics and Glass, Glass bank, http://glassbank.ifmo.ru.
[59] C.L. Wong, H.P. Ho, K.S. Chan, S.Y. Wu, and C. Lin, Application of spectral surface plasmon resonance to gas pressure sensing, Optical Engineering, vol. 44, pp. 124403, (2005).

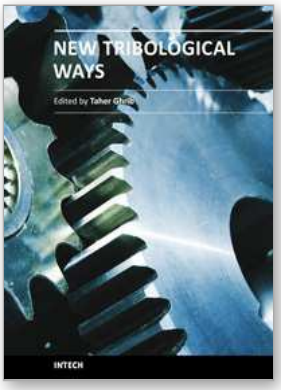

New Tribological Ways

Edited by Dr. Taher Ghrib

ISBN 978-953-307-206-7
Hard cover, 498 pages
Publisher InTech
Published online 26, April, 2011
Published in print edition April, 2011

This book aims to recapitulate old information's available and brings new information's that are with the fashion research on an atomic and nanometric scale in various fields by introducing several mathematical models to measure some parameters characterizing metals like the hydrodynamic elasticity coefficient, hardness, lubricant viscosity, viscosity coefficient, tensile strength .... It uses new measurement techniques very developed and nondestructive. Its principal distinctions of the other books, that it brings practical manners to model and to optimize the cutting process using various parameters and different techniques, namely, using water of high-velocity stream, tool with different form and radius, the cutting temperature effect, that can be measured with sufficient accuracy not only at a research lab and also with a theoretical forecast. This book aspire to minimize and eliminate the losses resulting from surfaces friction and wear which leads to a greater machining efficiency and to a better execution, fewer breakdowns and a significant saving. A great part is devoted to lubrication, of which the goal is to find the famous techniques using solid and liquid lubricant films applied for giving super low friction coefficients and improving the lubricant properties on surfaces.

How to reference

In order to correctly reference this scholarly work, feel free to copy and paste the following:

C.L. Wong, X. Yu, P. Shum and H.P. Ho (2011). Optical Characterization of Elastohydrodynamic Lubrication Pressure with Surface Plasmon Resonance, New Tribological Ways, Dr. Taher Ghrib (Ed.), ISBN: 978-953-307-206-7, InTech, Available from: http://www.intechopen.com/books/new-tribological-ways/optical-characterization-of-elastohydrodynamic-lubrication-pressure-with-surface-plasmon-resonance

INTECH
open science | open minds

InTech Europe
University Campus STeP Ri
Slavka Krautzeka 83/A
51000 Rijeka, Croatia
Phone: +385 (51) 770 447
Fax: +385 (51) 686 166
www.intechopen.com

InTech China
Unit 405, Office Block, Hotel Equatorial Shanghai
No.65, Yan An Road (West), Shanghai, 200040, China
中国上海市延安西路65号上海国际贵都大饭店办公楼405单元
Phone: +86-21-62489820
Fax: +86-21-62489821